Target Chamber Studies for a Light Ion Fusion Laboratory Microfusion Facility

B. Badger, R.R. Peterson, R.L. Engelstad, M.E. Sawan,
H. Khater, J.J. MacFarlane, G.A. Moses, E.G. Lovell

August 1988

UWFDM-768

FUSION TECHNOLOGY INSTITUTE

UNIVERSITY OF WISCONSIN

MADISON WISCONSIN

Target Chamber Studies for a Light Ion Fusion Laboratory Microfusion Facility

B. Badger, R.R. Peterson, R.L. Engelstad, M.E. Sawan, H. Khater, J.J. MacFarlane, G.A. Moses, E.G. Lovell

Fusion Technology Institute
University of Wisconsin
1500 Engineering Drive
Madison, WI 53706

http://fti.neep.wisc.edu

August 1988

UWFDM-768

TARGET CHAMBER STUDIES FOR A LIGHT ION FUSION LABORATORY MICROFUSION FACILITY

B. Badger, R.R. Peterson, R.L. Engelstad,
M.E. Sawan, H. Khater, J.J. MacFarlane,
G.A. Moses, E.G. Lovell

Fusion Technology Institute
University of Wisconsin-Madison
1500 Johnson Drive
Madison, WI 53706

August 1988

UWFDM-768

I. INTRODUCTION

A preliminary study of the target chamber design for a light ion beam driven Laboratory Microfusion Facility (LMF) has been completed. Four aspects of target chamber design have been studied: 1) deposition of target generated x-rays and ions in target chamber gases and structures, and the resulting vaporization of and pressure loading on the first wall, 2) response of the target chamber vessel to pressure loading and the design of target chamber walls, 3) induced radioactivity in target chamber walls and resulting dose rates, and 4) approximate cost of a target chamber. The analysis of these issues has been restricted to methods that were available at the beginning of the effort and limited to what could be accomplished in one month. Therefore, the results presented here represent a first attempt to address these issues.

It has been assumed that the LMF will explode fusion targets with yields between 10 and 1000 MJ over a period of 30 years as shown in Table 1.1. Yields of 10, 50, 200, and 1000 MJ have been used to represent the four ranges in Table 1.1. Studies began by fixing the radius of the target chamber at 1.5 m, allowing the option of increasing the radius if it became necessary. The diodes are roughly 4.0 m from the target and therefore it is believed that the maximum chamber radius is 3.0 m. There are advantages to the beam propagation in having the wall radius as small as possible. It was assumed that the beam ions are ballistically focussed onto the target, and therefore the target chamber fill gas was chosen to be 21 torr-meters of helium to limit the scattering of the beam ions. The possibility exists of adding up to 1 torr-meter of neon or nitrogen gas to help protect the target chamber wall from target x-rays. The target design from the LIBRA study[1] was used, based on a well-known target design from Lawrence Livermore National Laboratory.[2] The thermonuclear burn of this target[3] was simulated and it

is predicted that 22% of the target yield will be in x-rays with the spectrum shown in Fig. 1.1, and 6% will be in 550 keV target debris ions.

Table 1.1. LMF Shots Per Year Versus Target Yield

Operating Year	Yield			
	<10 MJ	10-100 MJ	100-500 MJ	1000 MJ
1-3	330	160	10	0
4-6	270	200	20	10
7-9	50	350	80	20
10-12	20	280	160	40
13-30	10	140	280	70
Total	2190	5490	5850	1470

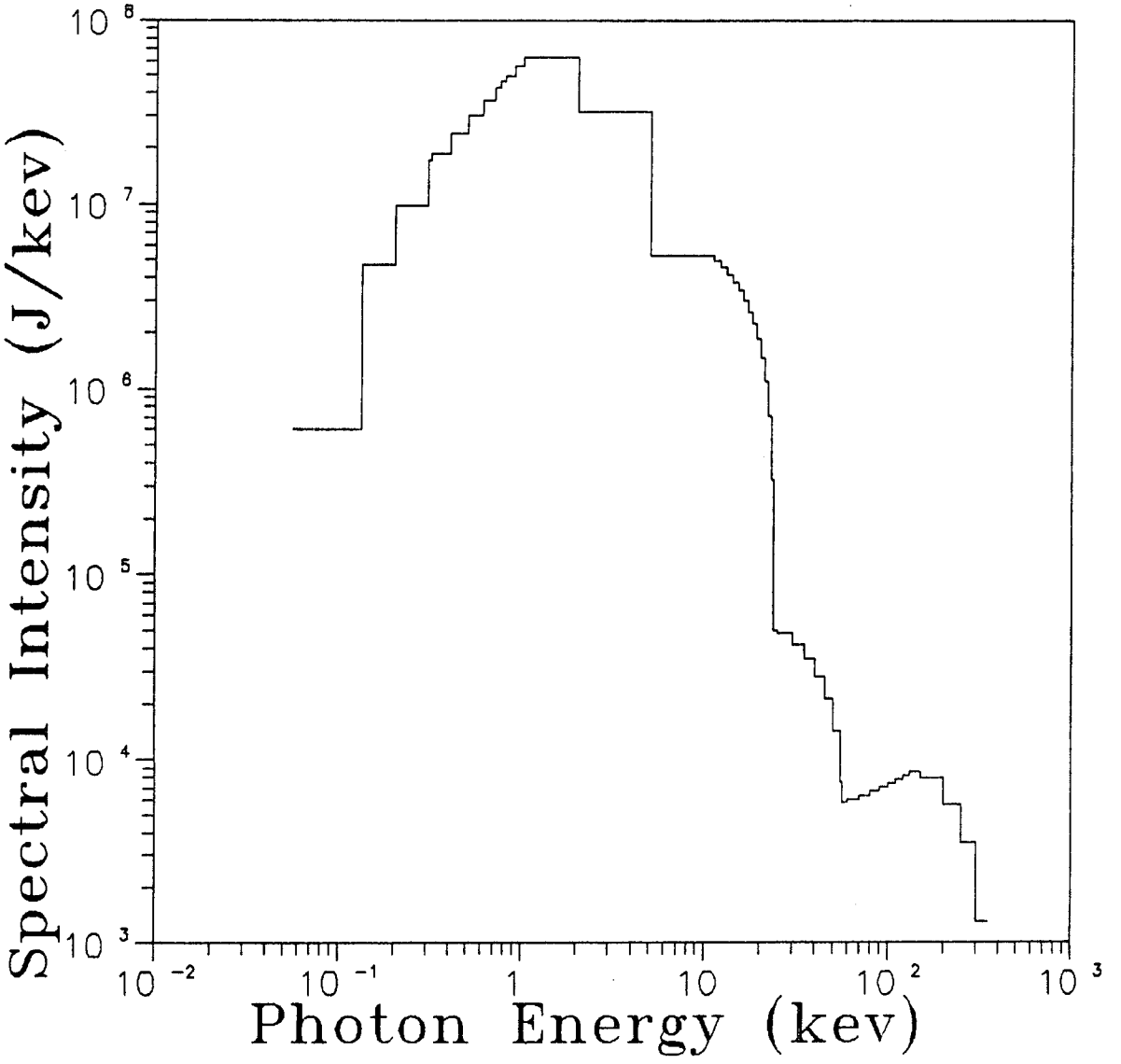

Fig. 1.1. Target x-ray spectrum for light ion beam fusion LMF target.

II. TARGET CHAMBER GAS RESPONSE

The CONRAD computer code[4] was used to simulate the behavior of target chamber gases under the influence of target generated x-rays and ions. CONRAD is a one-dimensional Lagrangian radiation hydrodynamics computer code that includes the effects of vaporization and condensation of wall material. The code models the deposition of a given spectrum of x-rays in the target chamber gas and in the walls in either a time-dependent or time-independent manner. The effect on the x-ray stopping power of depletion of the population of tightly-bound electrons in the background gas atoms is considered. The code also models the deposition of ions in a time-dependent manner, where the changing charge of the ions is taken into account.[5] These simulations are all for a target chamber 1.5 m in radius that is lined with graphite. These results have also been obtained under the assumption that the target chamber is spherical, though it will most probably be a cylindrical vessel that is capped on both ends. Since much of the wall is more than 1.5 m from the target, the calculations overestimate the mechanical loadings on the walls.

The general results of the studies in Fig. 2.1 show the mass of material vaporized from the first wall, peak pressure on the first wall, and impulse on the first wall versus the target yield. One can draw some conclusions from this plot that have importance to the overall target chamber design. For target yields of 50 MJ and higher there is first wall vaporization and the resulting peak pressures are at least several GPa. These peak pressures are large enough to generate shocks that move through the first wall, possibly damaging the wall. A solution to this problem, to be discussed in the recommendations at the end of this report, is to line the wall with some shock absorbing material that might have to be replaced between shots. One could lower the peak pressures somewhat by designing a target chamber with the

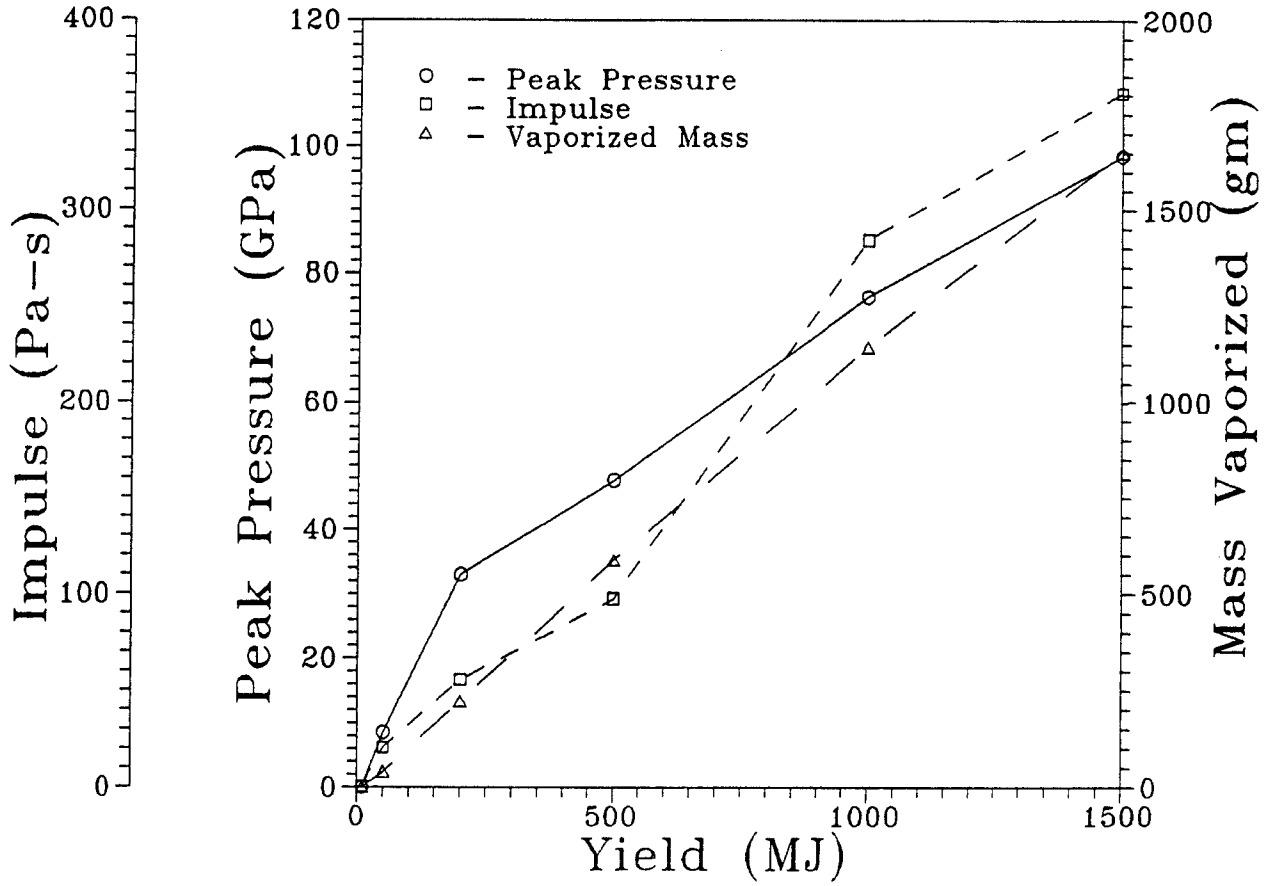

Fig. 2.1. Peak pressure, impulse, and mass vaporized for LMF versus target yield. The wall radius is 1.5 m and the target chamber fill gas is pure helium.

largest possible radius, 300 cm, but it is believed that with 1000 MJ yields the wall will still partially vaporize and peak pressures will still be in the 10's of GPa range. Below, the physics of wall vaporization is discussed to show how these high pressures are coupled to vaporization. In fact, one sees in Fig 2.1 that a strong correlation exists between the mass vaporized, the peak pressure and the impulse on the wall. The mass vaporized is nearly proportional to the target yield for values above the threshold level. The threshold yield for the onset of vaporization is between 10 MJ and 50 MJ for 1.5 m radius with a graphite surface. Near the threshold, the mass vaporized is not proportional to the yield. The exact threshold yield for the onset of vaporization has not yet been determined. The impulse, which is the critical parameter in determining the wall thickness required, generally increases with yield and vaporized mass. In CONRAD simulations, the zoning of the Lagrangian mesh must be optimized for each yield. This optimization was done for yields of 10, 50, 200, and 1000 MJ, the yields prescribed in the definition of this study. The simulations at 500 and 1500 MJ have not been optimized and that may be the reason why those impulses fall below the general curve of the optimized results. The general levels of the impulses are well below those obtained from scaling the Target Development Facility (TDF) results in yield and target chamber volume.[6] This is because the TDF had a high-Z target chamber gas that stopped most of the target x-rays in a short distance, creating a strong shock, while the current LMF design has a low density helium gas that does not strongly absorb the x-rays.

The physics of vaporization of material from the LMF first wall is important to the pressures and impulses experienced by the first wall. CONRAD has been used to study the behavior of the vapor immediately after vaporization by target x-rays. When a burst of x-rays is instantaneously deposited in

a layer of graphite, and the fluence is high enough to raise the energy density in a part of the material above that required for vaporization, that part of the material will then begin to ablate as a free vapor. The x-rays attenuate in the material exponentially, so, if the pulse width of the x-rays is shorter than the time for the vapor to move, a pressure profile will exist in the vapor that is peaked on the interface between the vapor and the target chamber fill gas. The simulations show that the pressure profile initiates shocks moving from the interface into the fill gas and through the vapor toward the intact solid wall. This is shown in Figs. 2.2, 2.3, and 2.4. These plots show some detail of the vaporization of graphite from a 1.5 m radius wall for a target yield of 1000 MJ. Fig. 2.2 shows the positions of Lagrangian zone boundaries versus time. One can clearly see the shock moving through the vapor and striking the wall. In Fig. 2.3, one sees the pressure profiles in the vapor. Initially, the exponential temperature profile leads to a sharply peaked pressure profile, which has a maximum value of 320 GPa. The peak pressure is reduced as the shock moves toward the wall, while the width spreads. The pressure at the first wall versus time is plotted in Fig. 2.4. The peak pressure on the wall occurs at about 5 ns. It is believed that the actual x-ray pulse should be about 1 ns wide, so perhaps the time-dependence of the x-ray deposition could be important, a fact that has so far been ignored. A CONRAD simulation has been done for time-dependent x-ray deposition and the same shock propagation has not been observed, but the peak pressure was still high at 63 GPa. Since the calculations show an attenuating shock moving through the vapor, the sensitivity of the results to radiation transfer coefficients and artificial viscosity has been tested and it has been found that changes in the radiation transfer do not greatly affect the peak pressures, but that increasing the artificial viscosity by a factor of then

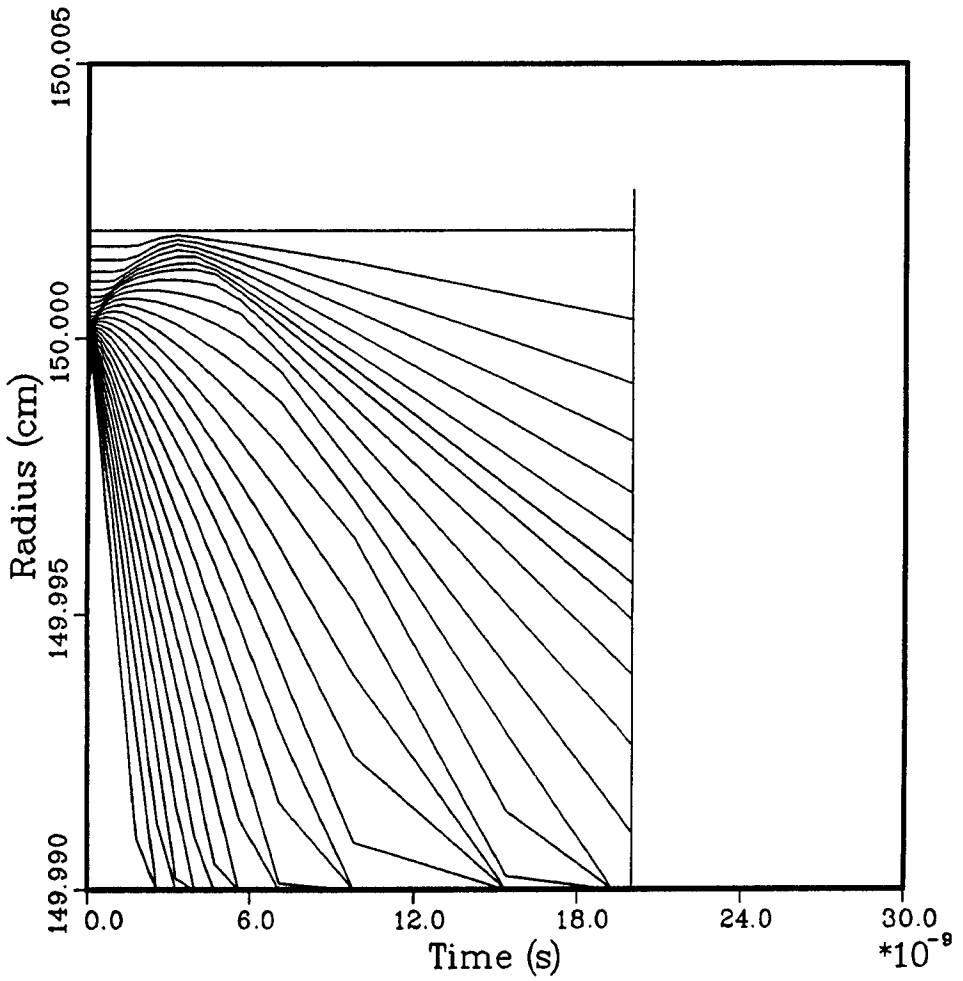

Fig. 2.2. Hydromotion of vaporized material. Target yield is 1000 MJ and other conditions are as in Fig. 2.1. X-ray deposition is instantaneous.

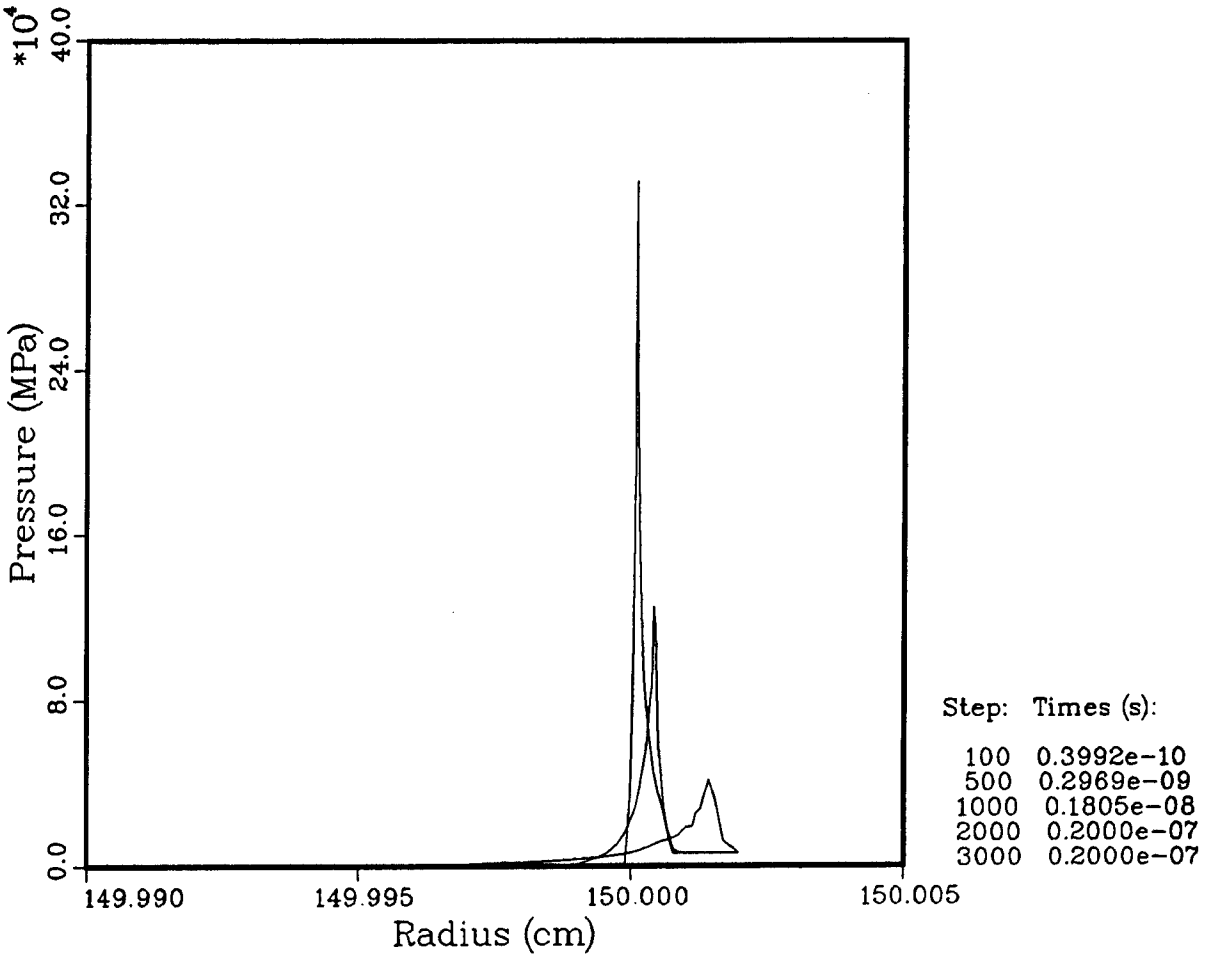

Fig. 2.3. Pressure profiles in vaporized material at various times. Target yield is 1000 MJ and other conditions are as in Fig. 2.1. X-ray deposition is instantaneous.

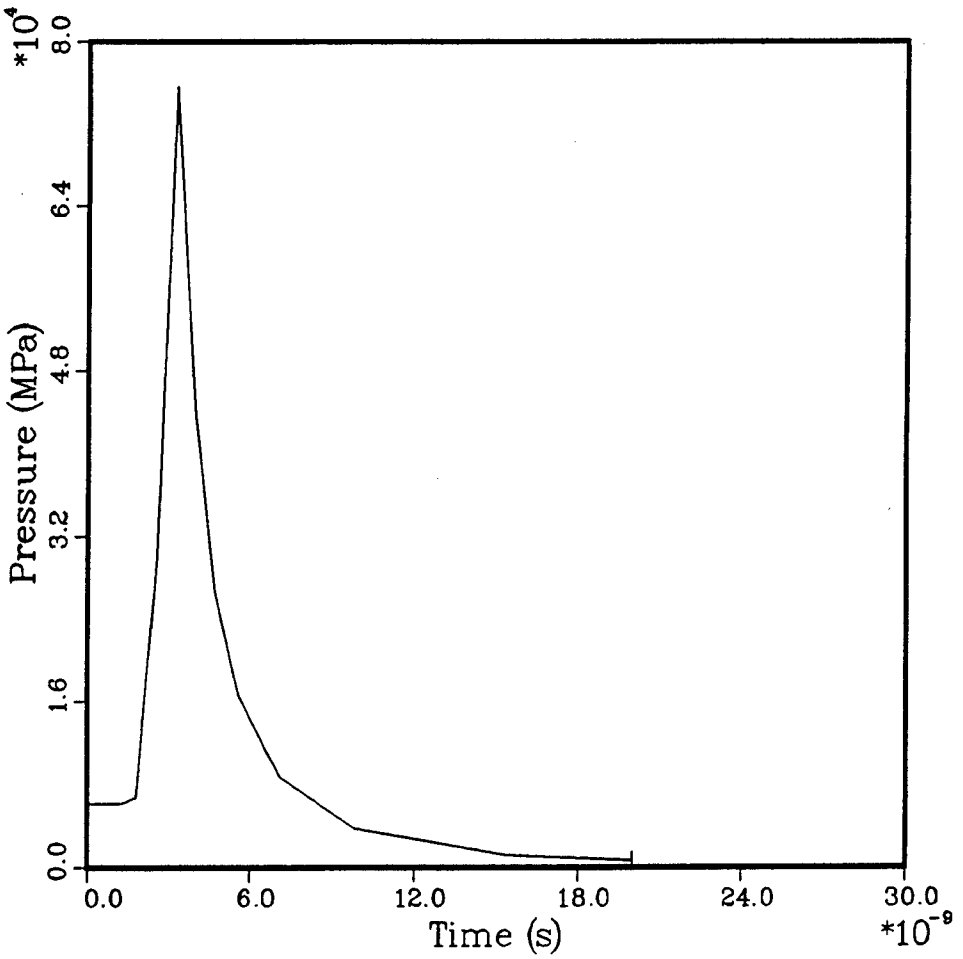

Fig. 2.4. Pressure at first wall versus time. Target yield is 1000 MJ and other conditions are as in Fig. 2.1. X-ray deposition is instantaneous.

decreases the peak pressure by a half. Finally, the motion of the vapor throughout the target chamber and how it interacts with the outward moving shock that is generated through the deposition of target ion debris has been examined. The hydromotion for the fill gas and the vapor is shown in Fig. 2.5, where it is seen that the vapor overwhelms the outward moving shock and that no shock reaches the wall after the one at 5 ns. The wall is therefore protected from the ordinary target generated blast wave by the vapor.

The behavior of target chamber gases with greater average-Z has also been considered. First, an attempt was made to absorb some x-rays by seeding the helium gas with 1 torr of neon or a mixture of 0.5 torr neon and 0.5 torr nitrogen. Neon and nitrogen have larger x-ray absorption coefficients than does helium, with the mixture being the best because the absorption peaks in nitrogen match the photon energies which have the weakest absorption in neon, and vice versa. However, it has been noticed that a 1000 MJ explosion releases 1.37×10^{24} photons, assuming the average photon energy to be 1 keV, while there are only 5×10^{23} neon or nitrogen atoms in the cavity. Therefore, depletion of the tightly-bound electrons in the nitrogen and neon atoms should greatly reduce the ability of the gas to stop x-rays. In fact, the CONRAD code accounts for this "bleaching" effect and does predict that neon and nitrogen will not protect the walls from the x-rays to any significant degree. Denser gases have also been considered to absorb the x-rays and protect the wall from x-ray vaporization. Ballistic ion propagation would not be possible in such a gas, but these calculations give an upper limit on the impulse experienced by the first wall. For a 1000 torr nitrogen gas, a 1000 MJ explosion will impose a peak pressure on the wall of 40 MPa, and an impulse of 2000 Pa-s.

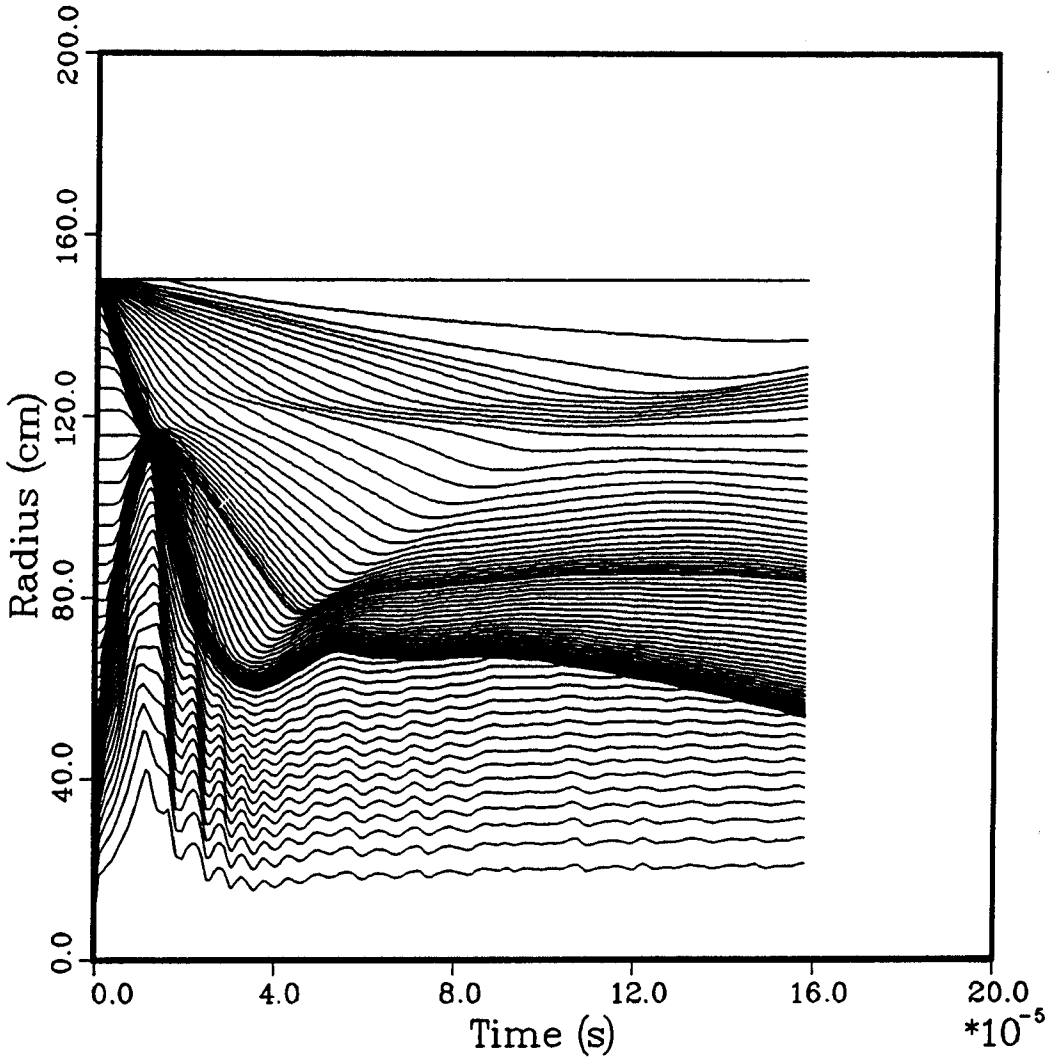

Fig. 2.5. Hydromotion of vaporized material and target chamber fill gas. Target yield is 1000 MJ and other conditions are as in Fig. 2.1. X-ray deposition is instantaneous.

III. MECHANICAL ANALYSIS OF THE TARGET CHAMBER

The chamber proposed for this LMF study consists of a capped cylindrical shell 1.5 m in radius and 4.5 m in length. While this is conceptually similar to the Target Development Facility (TDF), there are major differences as shown in Fig. 3.1. The cylindrical chamber of the proposed TDF has only a few small diameter beam ports. Thus the general stiffness characteristics and mechanical response will be virtually the same as an unperforated shell. Port stress concentration effects can be assessed and reduced with conventional design practices. In contrast with TDF, the LMF chamber is characterized by a large number of closely packed beam ports which will affect the overall response to dynamic loads.* A dynamic analysis of the vessel should be made by finite element methods. This was not within the scope of the present work.

The mechanical response and lifetime calculations of the LMF chamber have been analyzed with the assumption that the chamber can be modeled as a complete cylindrical shell. It has also been assumed that a sacrificial liner will be present in the chamber to absorb the substantial radial shock waves and, in addition, will act as a thermal barrier.

The chamber wall receives a severe pressure pulse which results in transient vibrations and stress. This response is primarily a function of the

---

*For the static case, plates or shells with continuous regular perforations can be analyzed satisfactorily with formulas for unperforated cases of equal size provided a virtual elastic modulus and virtual Poisson's ratio are used to compensate for the loss of stiffness and biaxial stress capacity. The average stress in the ligament is increased over that of the unperforated structure by the reciprocal of the ligament efficiency (ligament width/hole pitch). For the beam port pattern considered for the LMF chamber the efficiency is 54% and thus the average static stress in the ligaments would be increased by a factor of 1.85. Local stresses near the edge of the hole are larger but can be reduced with a reinforcing ring, designed to be approximately equal in volume to the hole and distributed on both sides of the wall if possible.

Target Development
Facility Chamber

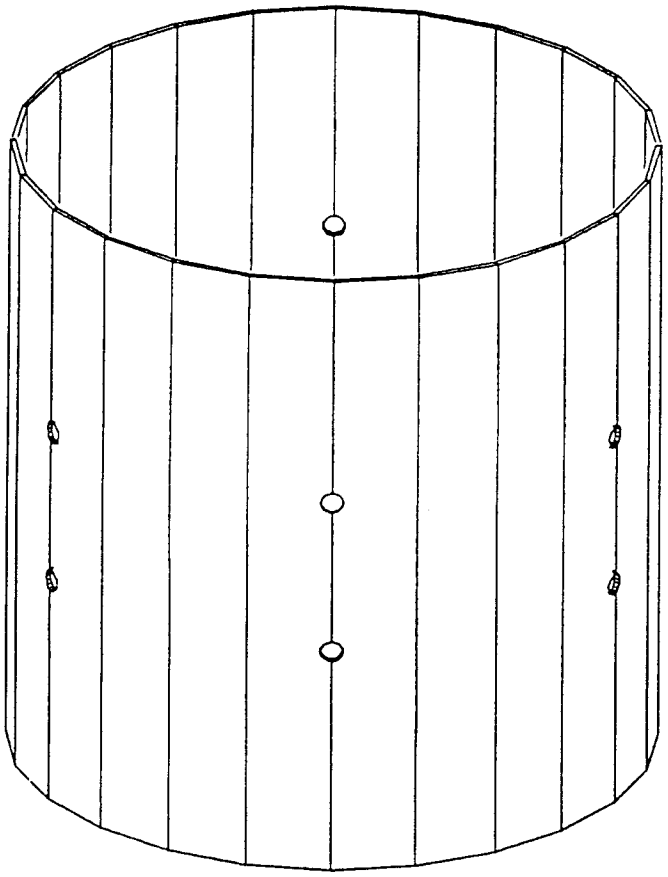

Radius: 3.0 m
Length: 6.0 m
No. of Beam Ports: 12
Beam Port Radius: 5.0 cm

Proposed LMF
Chamber Design

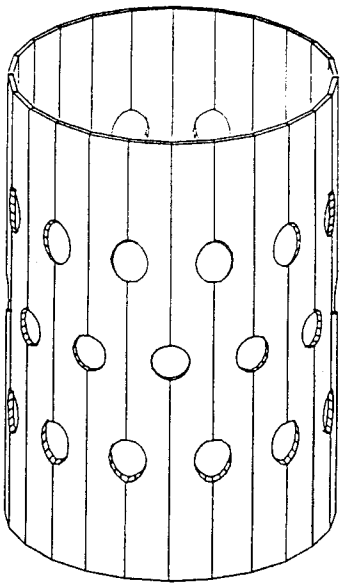

Radius: 1.5 m
Length: 4.5 m
No. of Beam Ports: 36
Beam Port Radius: 18.0 cm

Fig. 3.1. Chamber geometry comparisons.

impulse magnitude, i.e., practically independent of the shape of the pressure spike, providing the pulse width is considerably less than vibration periods of the chamber. (Additional stresses will be produced by static after-pressure, but such effects have not been considered in this analysis.) The pressure is assumed to be uniformly distributed over the surface. Thus the mechanical response is axisymmetric and also symmetric with respect to the midspan plane.

The largest stresses occur at the ends of the cylindrical chamber where it is supported. For example, Fig. 3.2 shows the flexural stress response of a 3 cm thick 2.25 Cr-1 Mo steel shell when a 284 Pa-s impulsive pressure is applied. These stresses are very concentrated and can be reduced by a local increase in wall thickness. Consequently, the design is based upon circumferential normal stress which is nearly uniform over most of the shell's length. A corresponding circumferential stress history is shown in Fig. 3.3. It should be noted that the stress histories for the steel and aluminum will be virtually identical since the ratio of the modulus to the density is the same for each. However, this is not the case for strains which can be seen in Figs. 3.4 and 3.5. Essentially, the strains in the aluminum are three times as large.

For fatigue-based design, cumulative damage must be assessed since each stress and strain history is characterized by cycles of different amplitudes and in addition, the individual history will also change as the target yield is increased. The procedure is consistent with the ASME Pressure Vessel Code,[7] but uses fully reversed alternating strain data as a function of number of cycles to failure. The code specifies a safety factor of two on strain or twenty on cycles, whichever is more conservative. A counting

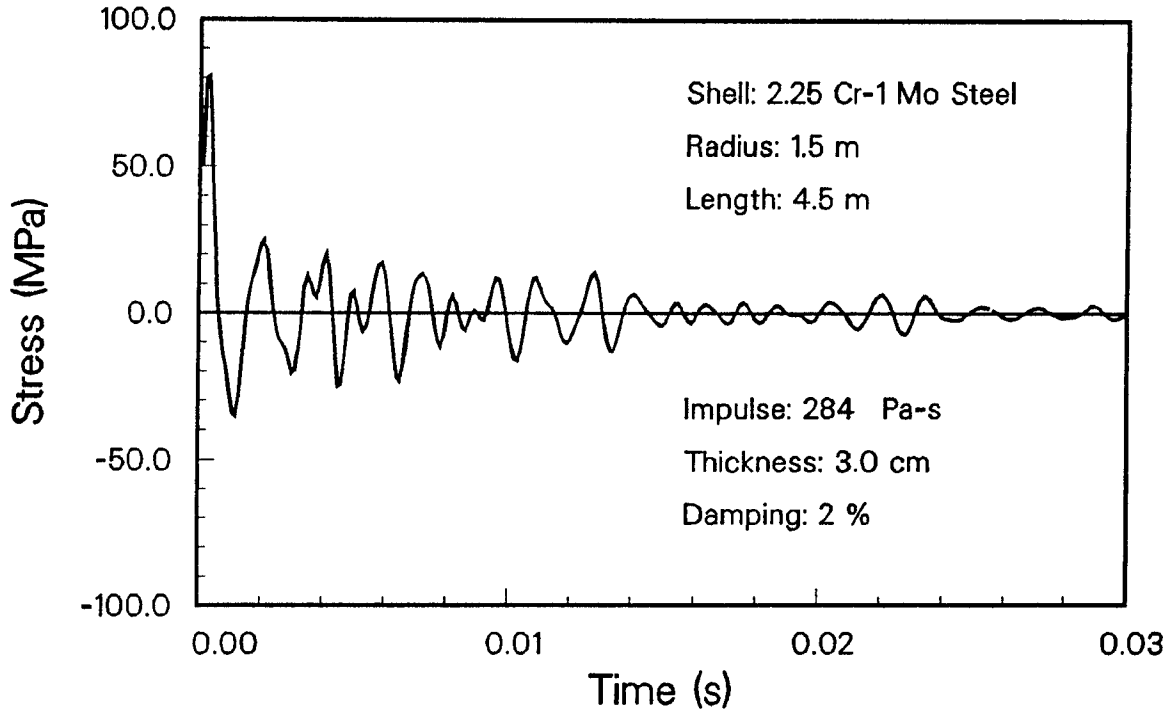

Fig. 3.2. LMF cylindrical shell flexural mechanical stress.

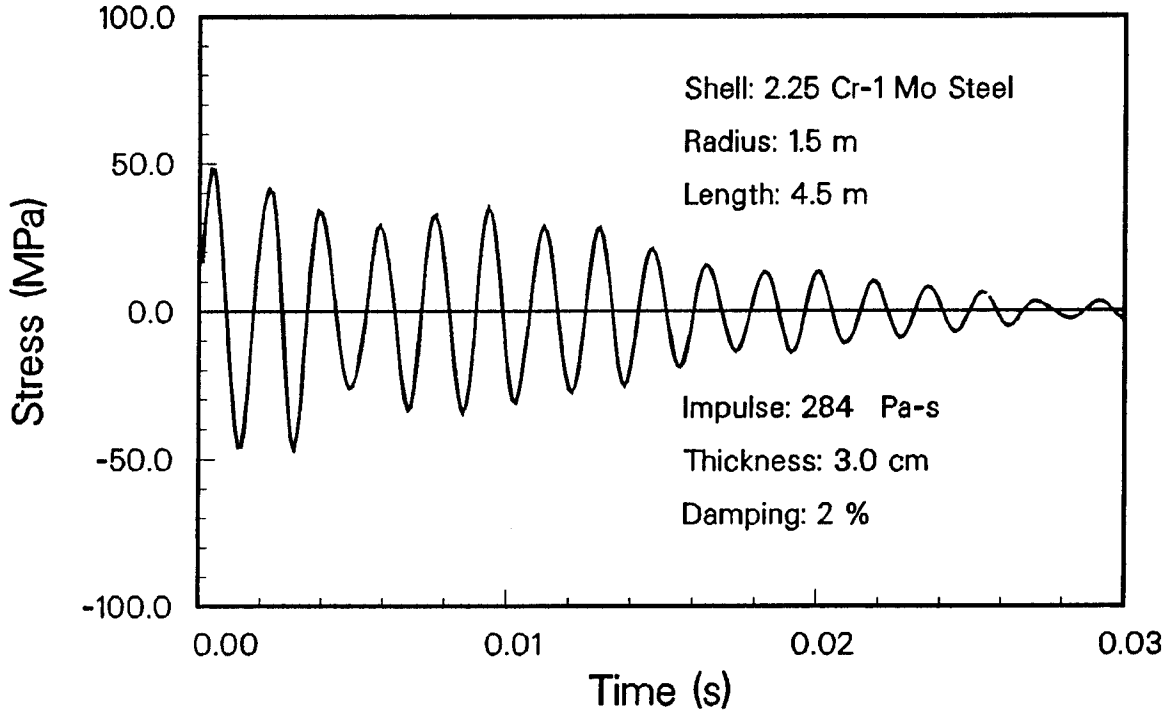

Fig. 3.3. LMF cylindrical shell circumferential mechanical stress.

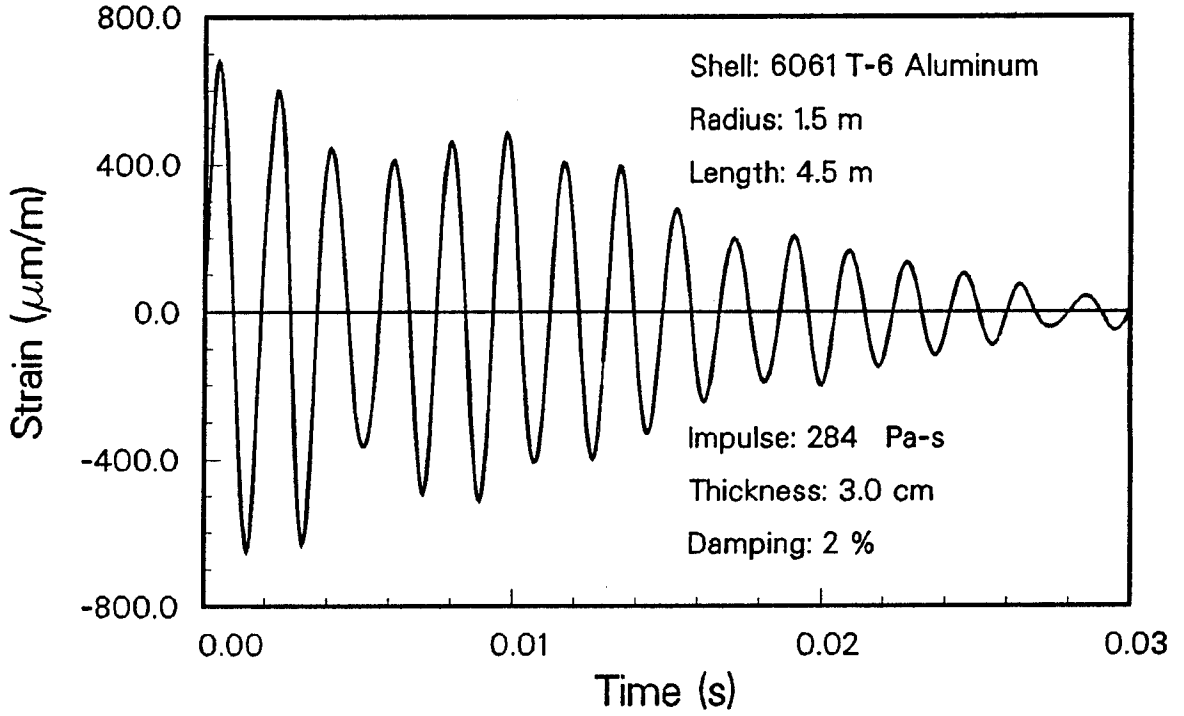

Fig. 3.4. LMF cylindrical shell circumferential mechanical strain (6061-T6 Al).

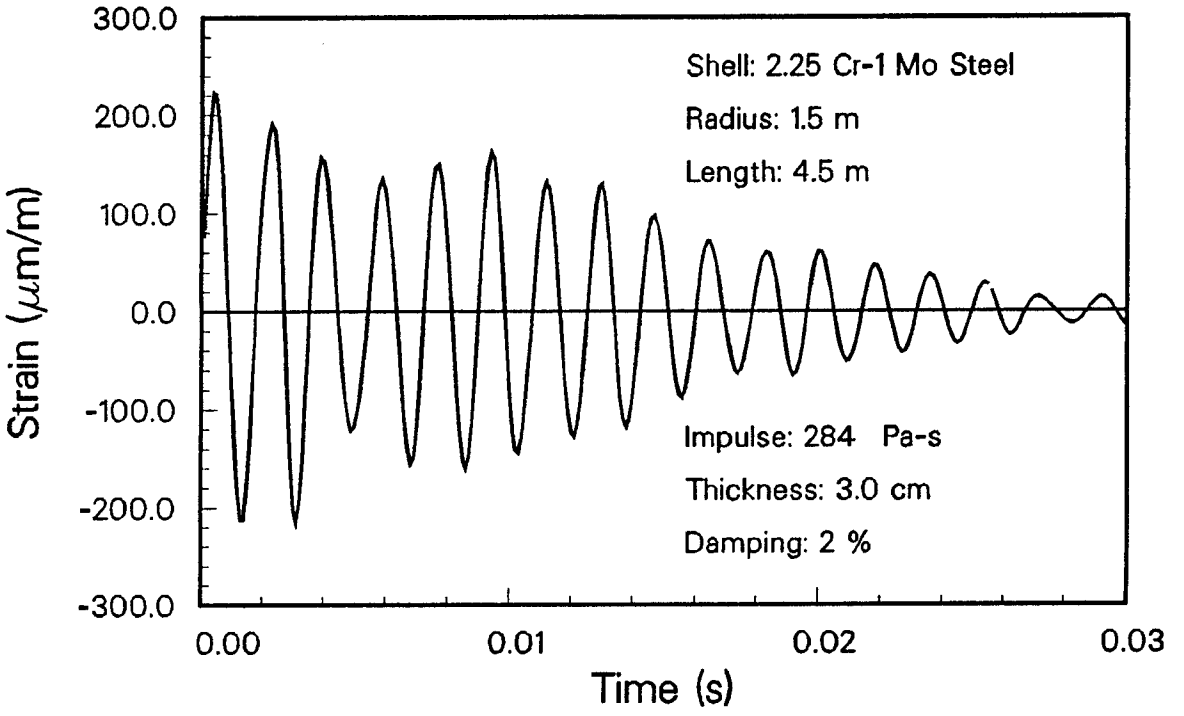

Fig. 3.5. LMF cylindrical shell circumferential mechanical strain (2.25 Cr-1 Mo).

technique is used for the histories in which cumulative damage is determined and compared with the materials' fatigue data. For a particular shell and loading schedule, the amount of damage can be assessed. The process can be repeated with different thicknesses until a minimum acceptable value is determined.

The fatigue strain data for 2.25 Cr-1 Mo, shown in Fig. 3.6 is from Booker et al., at ORNL.[8] These values were developed for nuclear steam generator designs and have been included in ASME Code Case N-47.[7] The data were obtained from completely reversed fixed-amplitude strain-controlled fatigue tests with the strain rate of 4×10^{-1}/s. The corresponding fatigue data for welded aluminum 6061-T6 were obtained from ASCE design codes.[9] A safety factor of 1.35 was originally built into the data. Cyclic tests of plate specimens have shown that a safety factor of at least 1.35 was provided by the ASCE guidelines. Consequently, the ASCE data were devalued by a factor of 1.35 and are shown in Fig. 3.7.

For the fatigue analysis, calculations were carried out for lifetimes of 3, 6, 9, 12 and 30 years. The cumulative shots used for each value of the target yield are shown in Table 3.1. Because of the relatively good fatigue life characteristics of 2.25 Cr-1 Mo steel, it was found that a very thin chamber wall could withstand a full lifetime of 30 years with a substantial factor of safety. Figure 3.8 shows the number of shots allowed of a particular target yield versus the corresponding impulsive pressure loading for various values of the thickness. A factor of safety of 2 has been included in the calculations to meet ASME code requirements. As an example, for a 3 cm thick wall, a lifetime of 40,000 shots of 1000 MJ can be sustained with a safety factor of 10. (It is recommended that a wall thickness of not

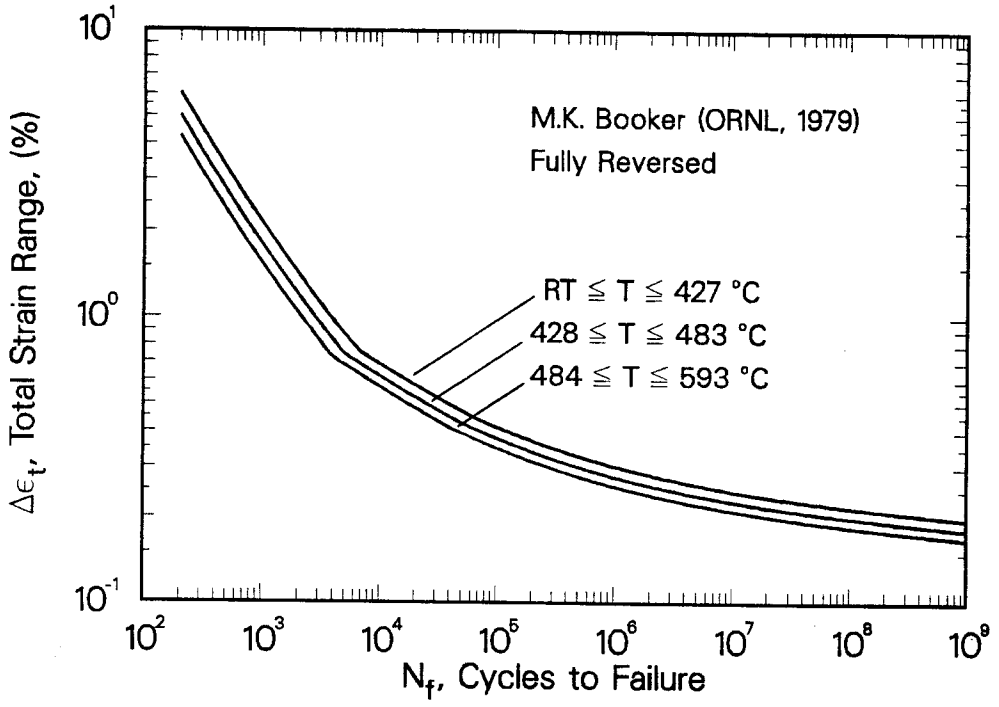

Fig. 3.6. Fatigue data for 2.25 Cr-1 Mo steel.

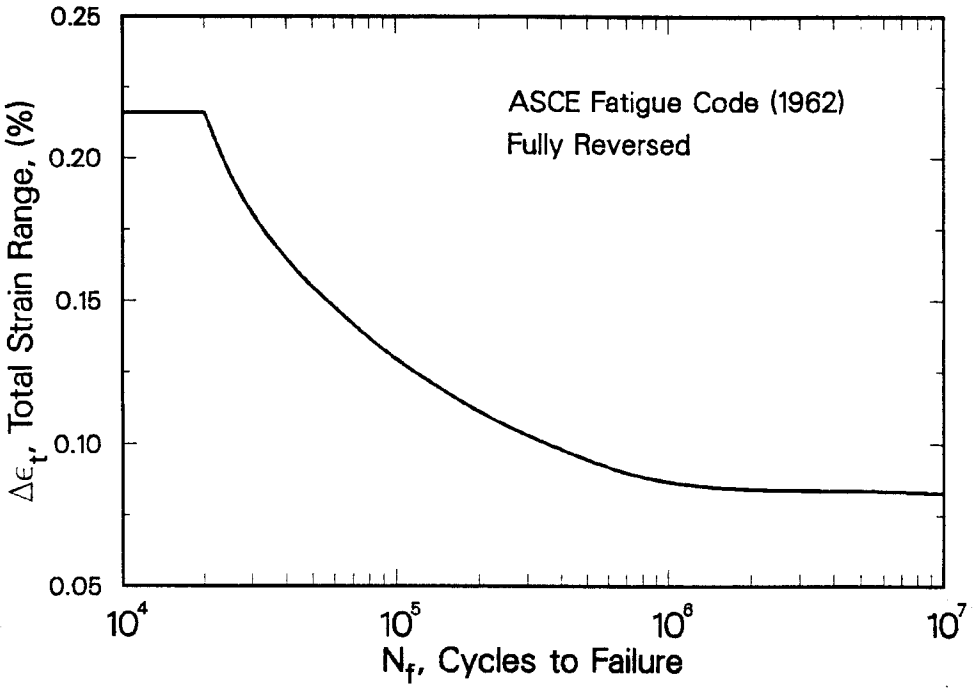

Fig. 3.7. Fatigue data for welded 6061-T6 aluminum.

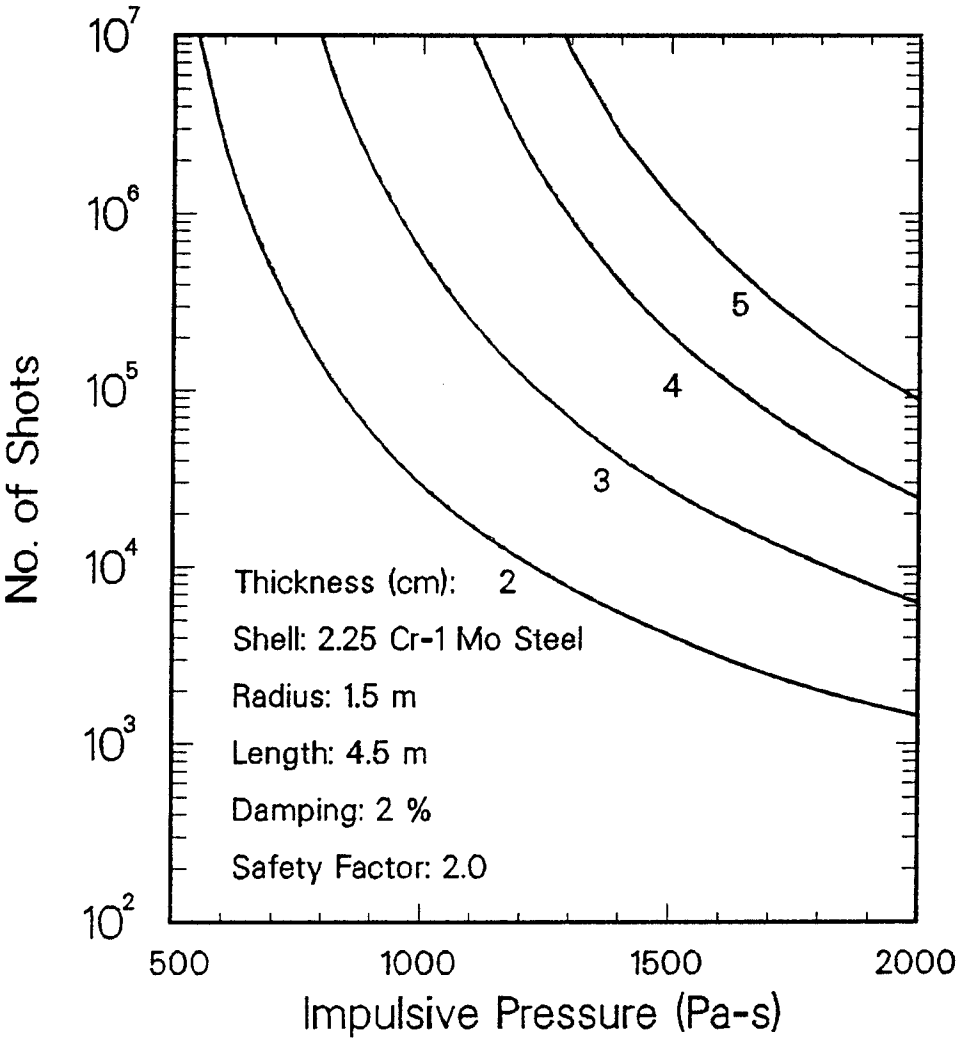

Fig. 3.8. Fatigue life of LMF cylindrical shell (2.25 Cr-1 Mo).

Table 3.1

LMF Cumulative Shots

Lifetime (Yrs)	10 MJ	50 MJ	200 MJ	1000 MJ
3	990	480	30	0
6	1800	1080	90	30
9	1950	2130	330	90
12	2010	2970	810	210
30	2190	5490	5850	1470

less than 3 cm be considered until a complete buckling analysis is done for the chamber.)

For the welded aluminum, fatigue calculations were governed by the impulsive load of 284 Pa-s from the 1000 MJ shot. With the fatigue curve being conservatively "flattened" for low cycles (Fig. 3.7), the failure mode is predominately yielding. Table 3.2 shows the minimum wall thickness needed at each lifetime for various factors of safety. It can be seen that in each case the value of the thickness remains the same for lifetimes of 6, 9, 12 and 30. However, the wall damage will scale directly with the number of 1000 MJ shots in each lifetime. Since there are no 1000 MJ shots included in a 3 year lifetime the wall thickness decreases substantially. Nevertheless, a minimum of 3 cm should still be considered here.

Table 3.2

LMF Chamber Fatigue Analysis
for 6061-T6 Aluminum

Safety Factor = 2

Lifetime (Yrs)	Minimum Thickness (cm)	Damage (%)
3	0.7*	0.47
6	3.6	0.60
9	3.6	1.80
12	3.6	4.19
30	3.6	29.35

Safety Factor = 3

Lifetime (Yrs)	Minimum Thickness (cm)	Damage (%)
3	1.1*	0.41
6	5.7	0.41
9	5.7	1.23
12	5.7	2.86
30	5.7	20.04

Safety Factor = 4

Lifetime (Yrs)	Minimum Thickness (cm)	Damage (%)
3	1.5*	0.41
6	7.4	0.40
9	7.4	1.20
12	7.4	2.80
30	7.4	19.58

*Thickness of 3 cm is recommended

IV. NEUTRONICS AND ACTIVATION ANALYSIS

IV.1 Calculational Procedure

Neutron transport calculations have been performed for the LMF chamber using the one-dimensional discrete ordinates code ONEDANT[10] together with the LANL MATXS5[11] cross section data library processed from the ENDF/B-V evaluated files. The standard LANL 30 neutron-12 gamma group structure was used. The problem has been modeled in spherical geometry with a point source at the center of the 1.5 m radius chamber. The energy spectrum of the neutrons emitted from the HIBALL target[12] was used to represent the source for the chamber calculations. The results are normalized to the average target yield of 200 MJ which corresponds to 7.1×10^{19} D-T fusions per shot. It should be pointed out that since shots of different yields are to be used in LMF, knowledge of the operational schedule before shutdown is essential for proper estimation of the dose after shutdown. The worst case conditions can be assessed by renormalizing the results to 1000 MJ assuming that the high yield shots will take place right before shutdown.

The calculations have been performed for two different chamber wall materials. The wall is 3 cm thick for the ferritic steel 2 1/4 Cr-1 Mo and 6 cm thick for the Al-6061-T6. In both cases a 2 cm thick graphite (H-451) liner is used on the inner surface of the chamber wall and a 1 cm thick sheet of boral (a B_4C-Al mixture) is placed on the outer surface of the wall. The target chamber is submerged in a borated water pool for neutron shielding. The borated water contains boric acid (H_3BO_3) at a concentration of 5 g/100 cm^3. The boron in both the borated water and boral is enriched to 90% ^{10}B for enhanced thermal neutron absorption. Schematics of the target chamber models used in the calculations are given in Fig. 4.1.

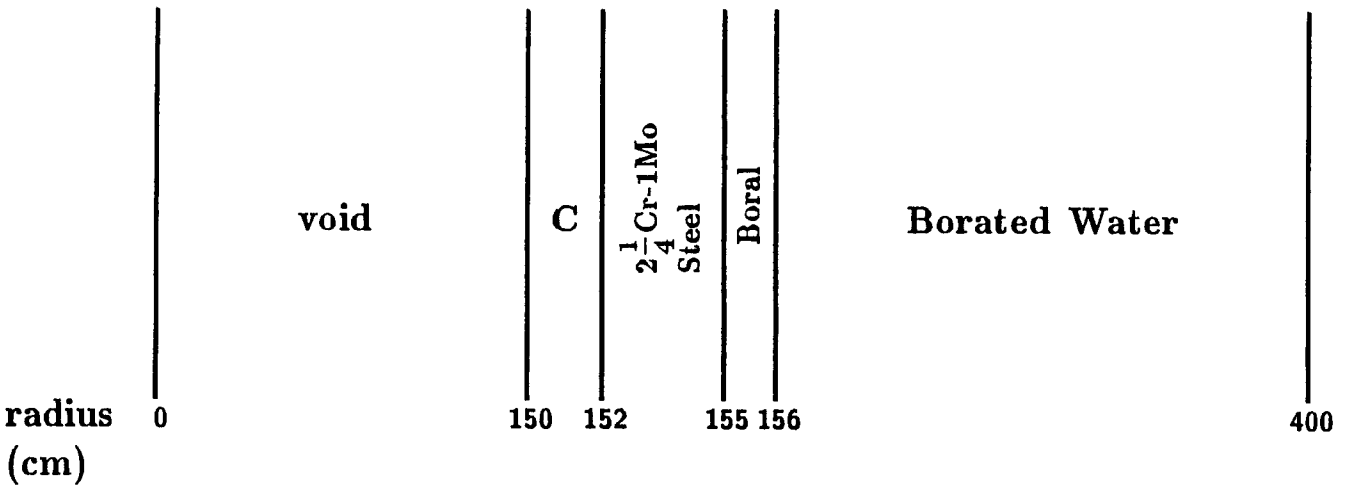

Steel Chamber

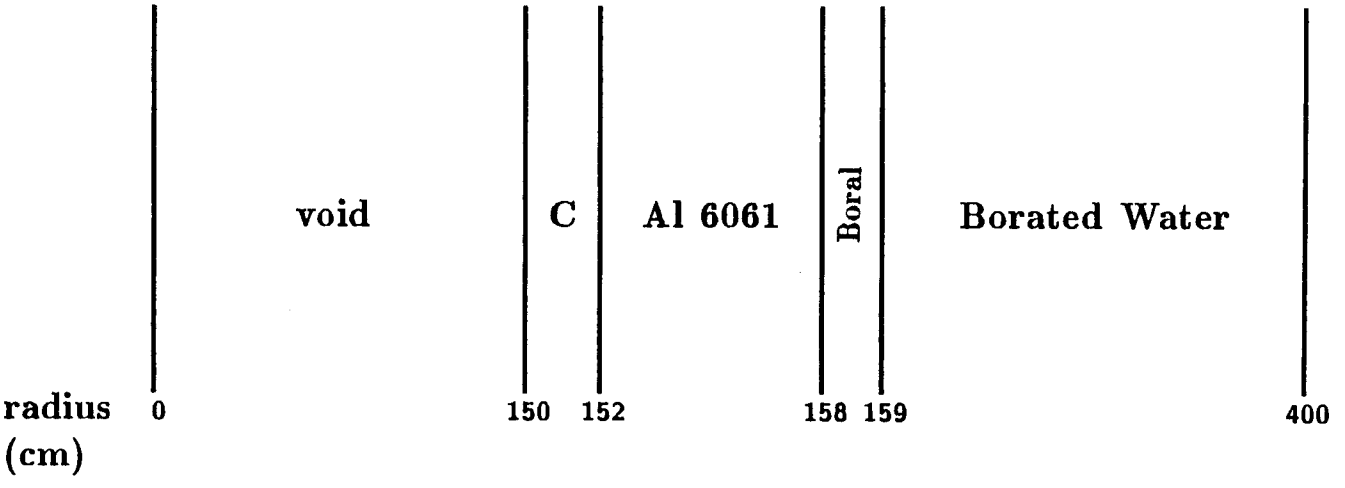

Al Chamber

Fig. 4.1. Schematic of the chamber models used in the calculations.

The neutron flux obtained from the neutron transport calculations has been used in the activation calculations. The radioactivity code DKR-ICF[13] has been used with the ACTL[14] neutron transmutation data library. The decay and gamma source data are taken from the Table of Isotopes.[15] The calculations have been performed for one year of operation with 500 shots. The pulsing schedule considered here allows for two shots per day which are 6 hours apart with 18 hours between the daily shots. Operating for 5 days a week results in 10 shots per week. Fifty weekly pulse sequences, which are 66 hours apart, are considered in the year. The DKR-ICF code gives the decay gamma source at different times following the final shot in the year. The adjoint dose field is then determined by performing a gamma adjoint calculation using ONEDANT with the flux-to-dose conversion factors representing the source at the point where the dose is to be calculated. The decay gamma source and the adjoint dose field are then combined to determine the dose at different times following shutdown. The contact dose at the outer surface of the boral layer was determined. In this case the borated water remains in place after shutdown. The dose was calculated also at a distance of 1 m outside the chamber wall for both cases with and without the borated water shield.

IV.2 Absorbed Dose in the Plastic Insulator

Since different plastic insulators will be used in LMF, an estimate of the expected end-of-life absorbed dose in such insulators is needed. This is required to determine the lifetime of the insulators and whether replacement is necessary during the 30 years of LMF operation. In the neutronics calculations a thin zone of a plastic insulator was used at the back of the boral layer and the absorbed dose was calculated using the appropriate kerma

factors. The composition of the plastic insulator used in the diode of TDF[16] was used in the calculations. It has a density of 0.95 g/cm^3 and has the chemical form $CH_2CHO_2CH_3$. The dose accumulated after 30 years of operation with 15,000 shots at an average yield of 200 MJ, has been calculated. The dose is 2×10^{10} rads for the aluminum chamber and 2.14×10^{10} rads for the steel chamber. The dose is slightly lower for the aluminum chamber due to the additional attenuation in the thicker aluminum wall. About 15% of the dose is due to the absorption of gamma photons produced in the wall. These values can be used to assess the lifetime of the plastic insulators in LMF. Notice that the absorbed dose results depend only on the cumulative yield and are independent of the schedule of the different yield pulses.

IV.3 Biological Dose After Shutdown

Figure 4.2 gives the contact dose at the outer surface of the LMF chamber as a function of time after shutdown. The results are given for both cases of aluminum and steel chamber walls. The number of shots was 500 at an average yield of 200 MJ. These calculations assume that the borated water shield will remain in place after shutdown. The results, therefore, represent the biological dose rate a diver would receive at the outer surface of the chamber. The dose rate for the aluminum chamber wall is larger than that for the steel wall up to approximately 3 days after shutdown while the steel dose is at least an order of magnitude higher than the aluminum dose over the period between one week and 5 years. In the case of the aluminum wall, the dose is dominated by ^{24}Na ($T_{1/2}$ = 15 hr), ^{27}Mg ($T_{1/2}$ = 9.5 min) and ^{28}Al ($T_{1/2}$ = 2.2 min) up to 10 min with ^{24}Na remaining as the main contributor up to 5 days. Between 5 days and 10 years the dominant radionuclides are ^{54}Mn

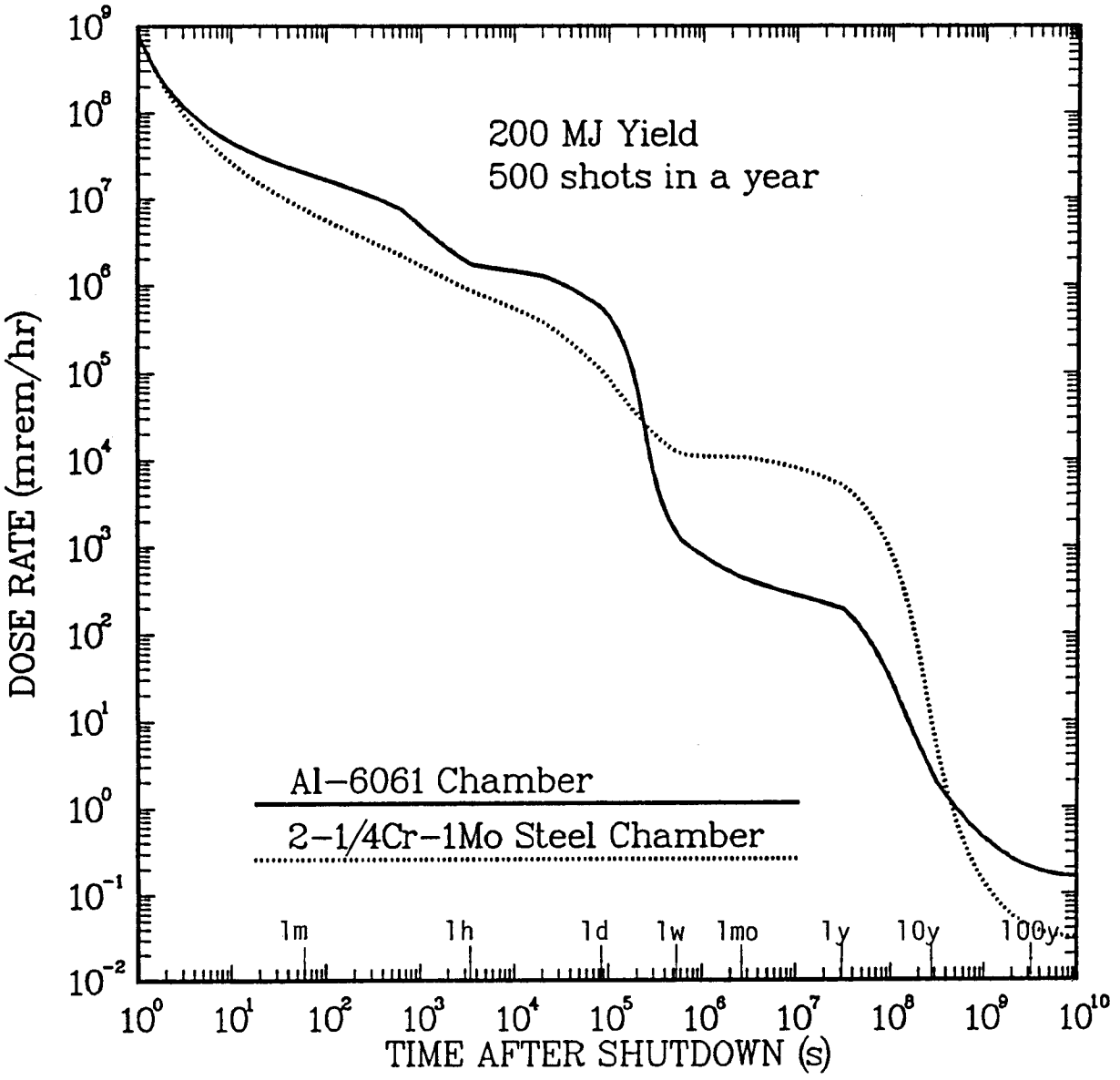

Fig. 4.2. Contact dose rate behind steel and Al chambers.

($T_{1/2}$ = 313 d) and ^{51}Cr ($T_{1/2}$ = 27.7 d). In the case of the steel wall, ^{28}Al and ^{56}Mn ($T_{1/2}$ = 2.6 hr) dominate the dose up to 10 min with ^{56}Mn remaining as the main contributor up to one day. In the period between one day and 10 years, ^{54}Mn and ^{51}Cr are the major contributors. The large drop in the aluminum dose level from 540 rem/hr at 1 day to 1.2 rem/hr at 1 week is the result of the decay of ^{24}Na which is produced by the ^{27}Al (n,α) reaction. The results indicate that one must wait approximately 1.5 years after shutdown for the aluminum case and about 5 years after shutdown for the steel case before the contact dose rate levels drop below 100 mrem/hr. This dose rate level allows a worker to work for 12.5 hours per quarter without receiving more than the allowable average quarterly dose of 1.25 rem.

Figure 4.3 compares the contact dose rate at the outer surface of the aluminum chamber to the dose rate at 1 m distance from the chamber. It is clear that a reduction in dose rate is achieved by limiting access for maintenance to a distance larger than 1 m from the chamber. If the borated water is drained out after shutdown, the dose rate is reduced by a factor of 2-3 in the period between 1 day and 1 week after shutdown and the dose rate will drop below 100 mrem/hr if one waits for only 2 weeks after shutdown. If the borated water shield is left in place after shutdown much lower dose rates will be obtained at all times except immediately after shutdown due to the ^{6}He ($T_{1/2}$ = 0.8 s) and ^{16}N ($T_{1/2}$ = 7.1 s) produced from activation of B and O in the borated water. In this case the dose rate drops to 100 mrem/hr after 3 days and to only 2.7 mrem/hr in one week following shutdown.

Table 4.1 lists the dose rate results obtained for the different cases considered. The results are given for 500 pulses each having the average yield of 200 MJ. As pointed out above, the dose in the first few days after

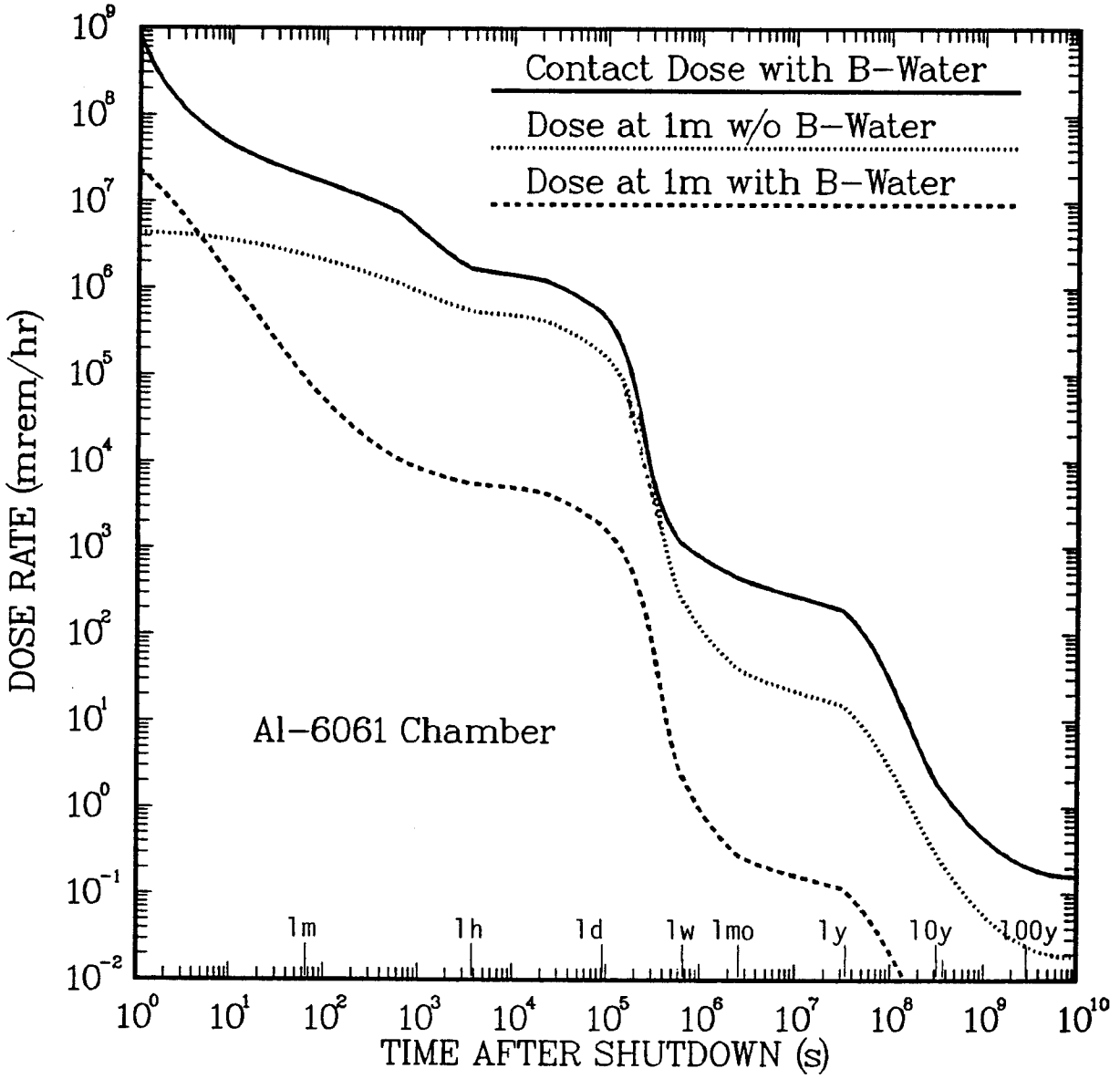

Fig. 4.3. Comparison between dose rates at the back of the Al chamber and at a distance of 1 m from the chamber.

shutdown is dominated by the short lived radionuclides ^{24}Na ($T_{1/2}$ = 15 hr) for the aluminum case and ^{56}Mn ($T_{1/2}$ = 2.6 hr) for the steel case. The activity levels for these nuclides after shutdown are determined only by the last few pulses before shutdown. The yield for these pulses has to be used to give a proper estimate of the dose in a few days following shutdown. The worst case estimate can be obtained by multiplying the results in Table 4.1 for t≤1 day by 5 to account for the possibility of having the last few pulses at a yield of 1000 MJ. On the other hand, after ~ 5 days following shutdown, the dose is dominated by the relatively long lived radionuclides ^{54}Mn ($T_{1/2}$ = 313 d) and ^{54}Cr (27.7 d). All shots during the year operation period will contribute to the activity of these radionuclides. Hence, for proper estimate of the dose rate in this period, the detailed temporal distribution of the different yield shots is required.

Table 4.1: Dose Rate (mrem/hr) Results for One Year Operation With 500 Shots and Average Yield of 200 MJ

Time After Shutdown	Contact Dose Rate		Dose Rate at 1 m from Al Chamber	
	2¼ Cr-1 Mo Steel	Al-6061	Borated Water Drained Out	Borated Water in Place
At Shutdown	8.52×10^{8}	8.53×10^{8}	4.34×10^{6}	2.36×10^{7}
1 min	7.47×10^{6}	2.01×10^{7}	2.43×10^{6}	9.39×10^{4}
1 hr	8.48×10^{5}	1.72×10^{6}	5.50×10^{5}	5.58×10^{3}
1 day	1.04×10^{5}	5.40×10^{5}	1.84×10^{5}	1.88×10^{3}
1 week	1.15×10^{4}	1.19×10^{3}	2.82×10^{2}	2.7
1 month	1.06×10^{4}	4.45×10^{2}	38.9	0.28
1 year	4.94×10^{3}	1.91×10^{2}	15.1	0.12
10 years	4.64	1.92	0.28	2.3×10^{-3}
Time for dose rate < 100 mrem/hr	5 yr	1.5 yr	2 wk	3 d
Time for dose rate < 2.5 mrem/hr	10 yr	7.5 yr	3 yr	1 wk

We conclude that while the aluminum chamber results in contact dose rate levels much lower than those for the steel chamber in the period between one week and 5 years after shutdown, one still has to wait several years for the dose rate to drop to tolerable levels. Limiting access for maintenance to distances greater than 1 m from the chamber allows maintenance to start in a few days after shutdown if the borated water remains in place. If the borated water is drained out maintenance can start after two weeks.

V. COSTS

Cost estimates for the LMF target chamber have been developed by comparing this target chamber with that designed for the light ion beam driven Advanced Pulse Experiment (APEX).[17] In the APEX study, the predicted cost of the target chamber was $226,000 in 1987 dollars for a 50 cm radius spherical chamber with 1 beam port and 35 diagnostic ports. The LMF will have 42 beams, so if the diagnostics are the same, the chamber will have 77 total ports. If 4% inflation is assumed and the cost scales as the complexity of the chamber, then the cost of the LMF chamber would be $500,000 in 1988 dollars. If, on the other hand, it is assumed that the cost is proportional to the surface area, the cost would be $2,938,000. In the APEX costing 85% of the materials costs were in quick disconnect valves and diagnostic port piping, which is proportional to the number of ports. It is also believed that labor costs should be close to proportional to the number of ports. Therefore, the estimated target chamber cost is $500,000. This does not include the cryogenic target system, the tritium control system, or the vacuum and gas handling system.

VI. RECOMMENDATIONS

On the basis of this analysis, the target chamber for the LMF could be built of 2 1/4 Cr-1 Mo steel at least 3 cm thick or aluminum 6061 at least 5 cm thick. This assumes that the chamber is a cylinder 1.5 m in radius, 4.5 m high, and is lined with a 2 cm thick graphite thermal shield on the inside and neutron absorbing boral layer on the outside. It is immersed in a pool of borated water to provide neutron and gamma shielding.

This design has been analyzed and it is believed that it could survive the shot schedule in Table 1.1, if a shock absorbing wall liner can be designed. If the ballistic beam focussing option is followed, a 12 torr pure helium fill gas is the best option. The activation of chamber wall is low enough after several days with the aluminum first wall to allow entry by divers into the borated water pool, though the actual dose rate will depend somewhat on the exact shot schedule. The cost of the target chamber is estimated to be $500,000.

Research issues remain on some areas of the target chamber design. An important consideration is the shock absorbing material on the wall. This material may need replacement before each shot and the environment inside the chamber will be highly radioactive until several days after the last shot. Therefore, the material would have to be replaced remotely. If the final LMF requirements include many large ports as in the preliminary concept, additional dynamic stress analysis is needed, including finite element calculations. Also, if the mechanical shock is typically characterized by an afterpressure, a revised strain cycle counting technique should be added to the fatigue code to assess mean stresses. Thick wall effects should be considered in the mechanical analysis if the chamber design evolves into a compact robust

configuration. The radioactive target debris in the target chamber, which represents perhaps 50% of the total radioactivity, has not been considered. This might be removed from the chamber, but a method for doing this has not been devised. The motion of radioactive target debris into penetrations in the target chamber is a concern that should be addressed. The target chamber has many holes and neutrons will find their way into these penetrations. These neutrons will activate material beyond the first wall, such as diodes, diagnostics, and the target injection system. Multi-dimensional neutronics and activation calculations are required to study this problem. The motion of vaporized material or blast waves into the beam ports has not been studied nor has the generation of vapor by x-rays striking the walls of the beam delivery tubes. Vapor from either source should be kept from the diodes. The general problem of condensation of the vapor should be addressed. Some parts of the chamber may be sensitive to vapor deposition and the vapor might not be in the form of graphite. Obviously, engineering of the gas handling, target delivery, waste disposal, and tritium handling systems is required.

ACKNOWLEDGEMENT

This work was performed for Sandia National Laboratory under contract number 55-6878. Computer support has been provided in part by the National Science Foundation at the San Diego Supercomputer Center.

REFERENCES

1. G.A. Moses, et al., "LIBRA - A Light Ion Beam Fusion Reactor Conceptual Design," University of Wisconsin Fusion Technology Institute Report UWFDM-787 (July 1988).

2. R.O. Bangerter and D. Meeker, "Ion Beam Inertial Fusion Target Designs," Lawrence Livermore Laboratory Report UCRL-78474 (1976).

3. B. Badger, et al., "HIBALL - A Conceptual Heavy Ion Beam Driven Fusion Reactor Study," University of Wisconsin Fusion Technology Institute Report UWFDM-450 (June 1981).

4. R.R. Peterson, J.J. MacFarlane, and G.A. Moses, "CONRAD - A Combined Hydrodynamics-Condensation/Vaporization Computer Code," University of Wisconsin Fusion Technology Institute Report UWFDM-670 (July 1988).

5. R.R. Peterson, et al., "Inertial Confinement Fusion Reactor Cavity Analysis: Progress Report for the Period 1 July 1987 to 30 June 1988," University of Wisconsin Fusion Technology Institute Report UWFDM-765 (July 1988).

6. B. Badger, et al., "Light Ion Beam Fusion Target Development Studies: Progress Report for the Period 1 November 1986 to 31 October 1987," University of Wisconsin Fusion Technology Institute Report UWFDM-752 (January 1988).

7. ASME Boiler and Pressure Vessel Code, Section III, Nuclear Power Plant Components.

8. M.K. Booker, J.P. Strizak, C.R. Brinkman, "Analysis of the Continuous Cycling Fatigue Behavior of 2.25 Cr-1 Mo Steel," Oak Ridge National Laboratory Report ORNL-5593, Oak Ridge, TN (1979).

9. "Suggested Specifications for Structures of Aluminum Alloys 6061-T6 and 6062-T6," Report of Task Committee on Lightweight Alloys, J. Str. Div. ASCE 88, ST6, 1095 (1962).

10. R. O'Dell et al., "User's Manual for ONEDANT: A Code Package for One-Dimensional, Diffusion-Accelerated, Neutral-Particle Transport," LA-9184-M, Los Alamos National Lab. (1982).

11. R. MacFarlane, "Nuclear Data Libraries from Los Alamos for Fusion Neutronics Calculations," Trans. Am. Nucl. Soc., 46, 271 (1984).

12. M. Sawan et al., "Nuclear Analysis of the Heavy-Ion-Beam-Driven Fusion Reactor HIBALL," Nucl. Technol./Fusion, 4, 79 (1983).

13. D. Henderson and O. Yasar, "DKR-ICF: A Radioactivity and Dose Rate Calculation Code Package," University of Wisconsin Fusion Technology Institute Report UWFDM-714 (1986).

14. M. Gordinier and R. Howerton, "ACTL: Evaluated Neutron Activation Cross Section Library Evaluation Techniques and Reaction Index," UCRL-50400, Vol. 18 (1978).

15. C.M. Lederer et al., Table of Isotopes, 6th and 7th Editions, Wiley (1967 and 1978).

16. D. Henderson, M. Sawan and G. Moses, "Radiological Dose Calculations for the Diode Region of the Light Ion Fusion Target Development Facility," Fusion Technology, 13, 594 (1988).

17. R. Whitley, et al., "Final Report for the APEX Target Chamber Preliminary Design Project," TRW Report SED.RW.87.092 (December 1987).